

AS-ITP-98-13
MADPH-98-1089

Scales, Couplings Revisited and Low Energy Phenomenology in M-theory on S^1/Z_2

Chao-Shang Huang¹, Tianjun Li², Wei Liao¹, Qi-Shu Yan¹

¹Institute of Theoretical Physics, Academia Sinica, P. O. Box 2735,
Beijing 100080, P. R. China

²Department of Physics, University of Wisconsin, Madison,
WI 53706, U. S. A.

Shou Hua Zhu

CCAST (World Lab), P.O. Box 8730, Beijing 100080, P.R. China
and Institute of Theoretical Physics, Academia Sinica, P. O. Box 2735,
Beijing 100080, P. R. China

Abstract

We revisit the eleven dimension Planck scale, the physical scale of the eleventh dimension, the physical scale of Calabi-Yau manifold and coupling in hidden sector in M-theory on S^1/Z_2 . And we discuss the reasonable bound on them. Considering F-term of dilaton and moduli SUSY breaking with the gaugino condensation in the hidden sector, we discuss the soft terms. We analyze experimental constraints to the parameter space in the dilaton dominant SUSY breaking scenario and the scalar quasi-massless scenario respectively. The sparticle spectrum and some phenomenological predictions are given.

October 1998

1 Introduction

In recent years revolutional progress in our understanding of string theories has been made. The key discoveries were dualities, which show that the five distinct superstring theories are in fact five different perturbative expansions of a single underlying theory (11-dimensional M theory or 12-dimensional F theory) about five different points in the moduli space of consistent vacua. The dualities, furthermore, show that in addition to the five points of the moduli space, there is a sixth special point in the moduli space which involves an 11-dimensional Minkowski space-time and is related to the strongly coupled heterotic (HE) and IIA superstring theories by compactifications on S^1/Z_2 and S^1 respectively [1]. Nowadays we do not have the complete picture of M theory so that one might argue that it is premature to make any attempt at phenomenology. However, experiences of investigating weak coupled $E_8 \times E'_8$ HE superstring phenomenology tell us that it may be that the corners of the moduli space capture most of the features of the theory relevant for low energy phenomenology.

Since Horava and Witten [2] described the strongly coupled $E_8 \times E'_8$ HE string theory by M-theory compactified on S^1/Z_2 whose low energy limit is the eleven-dimensional supergravity, many interesting phenomenology implications have been studied: Newton's constant and compactification, gluino condensation and supersymmetry breaking, Axions and Strong CP problem, threshold scale and strong coupling effects, proton decay, and phenomenological consequences [3, 4, 5, 6, 7, 8, 9, 10, 11, 12, 13, 14, 15, 16, 17, 18, 19, 20, 21, 22, 23, 24, 25] (for a review, see Ref. [26]). In short, all of above result seems to show that M-theory is a better candidate than previous weak-coupled heterotic string theory.

The most important one of discoveries of M theory phenomenology is that the discrepancy between the Grand Unification scale of around 2×10^{16} GeV estimated by extrapolating from the LEP measurements and the estimate of around 4×10^{17} GeV calculated in the weak coupled $E_8 \times E'_8$ HE string theory may be removed in the strongly coupled $E_8 \times E'_8$ HE string theory. In Horava and Witten's picture, at one end of the 11th dimensional line segment of length $\pi\rho$ live the observable fields contained in E_8 , at the other end live the hidden sector fields contained in E'_8 , and in the middle ('bulk') propagate the gravitational fields. One needs to consider further $R_4 \otimes X_{CY}$ (X_{CY} denotes a 6-dimensional Calabi-Yau manifold) compactification of 10-dimensional $E_8 \times E'_8$ HE string in order to get a realistic effective theory. Therefore, there are several scales and couplings such as the eleven dimension Planck scale, the physical scale of the eleventh dimension, the physical scale of Calabi-Yau manifold and the couplings in the observable and hidden sectors. The values of these scales and couplings and the relations between them have been estimated [12, 15].

Because the values of the scales and couplings are important for phenomenology and there are some issues which need to be discussed, In this paper we shall first revisit the eleven dimension Planck scale, the physical scale of the eleventh dimension, the physical scale of Calabi-Yau manifold and the coupling (in terms of the function x which is defined by $x = \frac{\alpha_H \alpha_{GUT}^{-1} - 1}{\alpha_H \alpha_{GUT}^{-1} + 1}$) in hidden sector in M-theory on S^1/Z_2 in standard embedding and non-standard embedding [23, 24, 25], and then discuss the possible bounds on them from the ansatz that the eleven-dimension Planck

scale is larger than the M_{GUT} , M_H which is the scale in the hidden sector just after the Calabi-Yau manifold is compactified, the eleventh dimension scale $[\pi\rho_p]^{-1}$. For the standard embedding, we obtain the upper bound on x is 0.97 ($x < 0.97$), for $\alpha_{GUT} = \frac{1}{25}$.

An important scale which is directly relevant to phenomenology is the scale Λ_{SUSY} from which the soft terms start running. There is a significant difference for Λ_{SUSY} between the weakly coupled and strongly coupled limits. In the weakly coupled limit Λ_{SUSY} is close to M_{Pl} since observable and hidden sector fields as well as gravitational fields all live in a same 10-dimensional space-time. In the strongly coupled limit, as Horava [4] has argued that SUSY breaking is not felt immediately in the observable sector because of a topological obstruction (the 11th dimension separates the two sectors). SUSY breaking in the hidden sector communicates to the observable sector by gravitational interactions. Therefore, SUSY breaking in the observable sector becomes apparent only after the renormalization scale Q is low enough to not reveal the presence of the 11th dimension anymore. Therefore, a natural and reasonable choice is $\Lambda_{SUSY} = [\pi\rho_p]^{-1}$. We estimate the value of $[\pi\rho_p]^{-1}$ and get its low bound of 9.5×10^{13} GeV.

In order to discuss the M-theory low energy phenomenology, we may need to pay attention to the supersymmetry breaking in M-theory and think about M-theory model building (essentially compactifications of 6-dimensional space-time), which is similar to what happened 10 years ago. As we know, we can discuss the supersymmetry breaking in the following ways: non-zero F-terms of the dilaton or moduli fields break the SUSY in which we do not specify the trigger of the SUSY breaking [15, 18, 19] or, maybe, gaugino condensation in the hidden sector [14], and the Scherk-Schwarz mechanism on the eleventh (or fifth) dimension (or we might call it coordinate-dependent compactification) [8, 9]. In this paper we consider the phenomenology in non-zero F-terms of the dilaton and/or moduli SUSY breaking with gaugino condensation in the Hidden sector [14]. There are a lot of papers to discuss compactifications in M theory on S^1/Z_2 [9, 12, 13, 19, 15]. It seems that the T^6/Z_{12} model is probably more close to the realistic one because it has three families. As pointed out below, it has the same soft terms as those in the simplest compactification under some reasonable approximations [14]. And from the point of phenomenological view, the important features of M theory phenomenology which are different from the weakly coupled limit and independent of the details of M theory model building are of unification of couplings and the magnitude of Λ_{SUSY} and the emphases of this paper are investigating characteristic features of low energy phenomenology of M theory. So in this paper we take the simplest compactification as an example (like most of people did) to discuss the soft terms. Then we calculate the low-energy sparticle spectrum under the LEP experiment constraints and discuss its dependence on Λ_{SUSY} . It is found that $M_{1/2}$ can not be larger than 420 GeV if one demands that masses of sparticles are not beyond 1 TeV. We analyze the constraints to the parameter space from $b \rightarrow s\gamma$. It is found that in the dilaton dominant SUSY breaking scenario although $b \rightarrow s\gamma$ imposes stringent constraints to the parameter space there still is a region of the parameter space where $\tan\beta$ is large and $M_{1/2}$ is small, which will lead to significant SUSY effects in some processes.

In this paper, we discuss the scales and couplings in the section 2. In section

3, we discuss soft terms. In section 4 we calculate sparticle spectrum using revised ISAJET. Section 5 is devoted to analyze the constraints from $b \rightarrow s\gamma$. We discuss the rare decay $B \rightarrow X_s\tau^+\tau^-$ and search of Higgs bosons in section 6. Finally, section 7 contains our conclusion.

2 Eleventh Dimension Scale and Gauge Coupling in Hidden Sector.

First, let's consider the gauge couplings, gravitational coupling and the physical eleventh dimension radius in the M-theory. The relative 11-dimensional Lagrangian is given by [2]

$$L_B = -\frac{1}{2\kappa^2} \int_{M^{11}} d^{11}x \sqrt{g} R - \sum_{i=1,2} \frac{1}{2\pi(4\pi\kappa^2)^{\frac{2}{3}}} \int_{M_i^{10}} d^{10}x \sqrt{g} \frac{1}{4} F_{AB}^a F^{aAB}. \quad (1)$$

In the 11-dimensional metric ¹, the gauge coupling and gravitational coupling in 4-dimension are [3, 12]:

$$8\pi G_N^{(4)} = \frac{\kappa^2}{2\pi\rho_p V_p}, \quad (2)$$

$$\alpha_{\text{GUT}} = \frac{1}{2V_p(1+x)} (4\pi\kappa^2)^{2/3}, \quad (3)$$

$$\alpha_H = \frac{1}{2V_p(1-x)} (4\pi\kappa^2)^{2/3}, \quad (4)$$

where x is defined by:

$$x = \pi^2 \frac{\rho_p}{V_p} \frac{\kappa}{4\pi} \int_X \omega \wedge \frac{tr F \wedge F - \frac{1}{2} tr R \wedge R}{8\pi^2}, \quad (5)$$

where ρ_p , V_p are the physical eleventh dimension radius and Calabi-Yau manifold volume (which is defined by the middle point Calabi-Yau manifold volume between the observable sector and the hidden sector) respectively, and $V_p = V e^{3\sigma}$ where V is the internal Calabi-Yau volume (For detail, see Ref. [12]). From above formula, we can obtain that:

$$x = \frac{\alpha_H \alpha_{\text{GUT}}^{-1} - 1}{\alpha_H \alpha_{\text{GUT}}^{-1} + 1}. \quad (6)$$

The GUT scale M_{GUT} and the hidden sector scale M_H when the Calabi-Yau manifold is compactified are:

$$M_{\text{GUT}}^{-6} = V_p(1+x), \quad (7)$$

¹Because we think 11-dimension metric is more fundamental than string metric and Einstein frame, we discuss the scales and couplings in 11-dimension metric.

$$M_H^{-6} = V_p(1-x) , \quad (8)$$

or we can express the M_H as:

$$M_H = \left(\frac{\alpha_H}{\alpha_{GUT}}\right)^{1/6} M_{GUT} = \left(\frac{1+x}{1-x}\right)^{1/6} M_{GUT} . \quad (9)$$

Noticing that $M_{11} = \kappa^{-2/9}$, we have

$$M_{11} = \left[2(4\pi)^{-2/3} \alpha_{GUT}\right]^{-1/6} M_{GUT} . \quad (10)$$

And we can also obtain the physical scale of the eleventh dimension in the eleven-dimensional metric:

$$[\pi\rho_p]^{-1} = \frac{8\pi}{1+x} (2\alpha_{GUT})^{-3/2} \frac{M_{GUT}^3}{M_{Pl}^2} . \quad (11)$$

Now, we consider constraints. Our ansatz is that the scale of M_{GUT} , M_H and $[\pi\rho_p]^{-1}$ should be lower than the eleven dimension Planck scale. From the constraints M_{GUT} and M_H is smaller than the scale of M_{11} , we obtain that:

$$\alpha_{GUT} \leq \frac{(4\pi)^{-2/3}}{2} ; \alpha_H \leq \frac{(4\pi)^{-2/3}}{2} , \quad (12)$$

or

$$\alpha_{GUT} \leq 2.7 ; \alpha_H \leq 2.7 , \quad (13)$$

they are independent number and large enough for our discussion. For the standard embedding, we obtain the upper bound on x is 0.97 ($x < 0.97$), for $\alpha_{GUT} = \frac{1}{25}$. From the constraints that $[\pi\rho_p]^{-1}$ is smaller than the scale of M_{11} , we obtain that:

$$M_{GUT}\alpha_{GUT}^{-2/3} \leq \sqrt{1+x} 2^{1/6} (4\pi)^{-4/9} M_{Pl} , \quad (14)$$

which is obviously satisfied for standard embedding. However, if we can consider non-standard embedding $x < 0$ [23, 24, 25], i. e., the gauge coupling in the observable sector is larger than the coupling in the hidden sector, we will have the following low bound on x:

$$x_{lb} \geq 2^{-1/3} (4\pi)^{8/9} (\alpha_{GUT})^{-4/3} \frac{M_{GUT}^2}{M_{Pl}^2} - 1 . \quad (15)$$

Right now, there exist three possibilities between the physical scale of the eleventh dimension and the physical scale of the Calabi-Yau manifold: $[\pi\rho_p]^{-1}$ is smaller than M_{GUT} and M_H which, from low energy to high energy, corresponds to from 4-dimension to 5 dimension and then, to 11-dimension; $[\pi\rho_p]^{-1}$ is smaller than M_{GUT} but larger than M_H , which, assuming x^{11} is the coordinate of the eleventh dimension, and the observable sector is at $x^{11} = 0$ plane and the hidden sector at $x^{11} = \int dx^{11} \sqrt{g_{11,11}}$ or the opposite plane, from low energy to high energy, corresponds to at one particular point x_c^{11} , from 4 dimension to 11 dimension directly, for $x^{11} < x_c^{11}$, from

4-dimension to 5 dimension and then, to 11-dimension, and for $x^{11} > x_c^{11}$, from 4-dimension to 10 dimension and then, to 11-dimension; $[\pi\rho_p]^{-1}$ is larger than M_{GUT} and M_H which, from low energy to high energy, corresponds to from 4-dimension to 10 dimension and then, to 11-dimension. Let us define the x_H and x_O which correspond to $[\pi\rho_p]^{-1} = M_H$ and $[\pi\rho_p]^{-1} = M_{GUT}$ respectively.

$$\left[\frac{(1+x_H)^7}{1-x_H} \right]^{1/6} = 8\pi(2\alpha_{GUT})^{-3/2} \frac{M_{GUT}^2}{M_{Pl}^2} , \quad (16)$$

$$x_O = 8\pi(2\alpha_{GUT})^{-3/2} \frac{M_{GUT}^2}{M_{Pl}^2} - 1 . \quad (17)$$

It is obvious that from eq. (11) when x decreases, $[\pi\rho_p]^{-1}$ increases if we consider specific α_{GUT} and M_{GUT} , so, we have $x_H \geq x_O \geq x_{lb}$.

Now we can discuss the numerical result. We take $M_{GUT} = 2.0 \times 10^{16}$ GeV, $\alpha_{GUT} = \frac{1}{25}$, $M_{Pl} = 2.4 \times 10^{18}$ GeV, then, we obtain the $M_{11} = 4.04 \times 10^{16}$ GeV, $x_{lb} = -0.96$, $x_O = -0.92$, $x_H = -0.878$, $[\pi\rho_p]^{-1}$ is from 7.8×10^{14} GeV to 1.5×10^{15} GeV when we vary x from 0 to 0.97 in the mean time for the standard embedding. If we choose the M_{GUT} is 3×10^{16} GeV, we obtain $M_{11} = 6.05 \times 10^{16}$ GeV, $x_{lb} = -0.91$, $x_O = -0.826$, $x_H = -0.758$, $[\pi\rho_p]^{-1}$ is from 2.64×10^{15} GeV to 5.2×10^{15} GeV when we vary x from 0 to 0.97 in the mean time. And we notice that x_{lb} , x_O , x_H increase if we increase the M_{GUT} . Therefore, if we had large GUT scale because of additional matter fields in the future M-theory model building, we might need to pay attention to x_{lb} , x_O , x_H in order to get clear picture of the universe.

Furthermore, we can discuss the possible low energy scale of $[\pi\rho_p]^{-1}$ which is interesting for the low energy phenomenology when $x > 0$ for standard embedding. Let us define the relation between the physical Calabi-Yau manifold volume and the unification scale M_{GUT} as in [15]:

$$aM_{GUT}^{-1} = (V_p(1+x))^{1/6} . \quad (18)$$

where $a > 1$. And a is smaller than 2.02 in order to keep the $M_{GUT} < M_{11}$ if we take $\alpha_{GUT} = \frac{1}{25}$. The formula is similar to above except the transformation: $M_{GUT} \rightarrow \frac{M_{GUT}}{a}$. Taking $M_{GUT} = 2.0 \times 10^{16}$ GeV, $\alpha_{GUT} = \frac{1}{25}$, $M_{Pl} = 2.4 \times 10^{18}$ GeV, we get the low bound on $[\pi\rho_p]^{-1}$ is 9.5×10^{13} GeV. Using $M_{GUT} = 3.0 \times 10^{16}$ GeV, the low bound is 3.2×10^{14} GeV. It follows that $\Lambda_{SUSY} \geq 10^{14}$ GeV, which is consistent with the estimate given in the Ref.[15].

3 Soft terms

The kähler potential, gauge kinetic function and the superpotential in the simplest compactification of M-theory on S^1/Z_2 are [15, 17]²:

$$K = \hat{K} + \tilde{K}|C|^2 , \quad (20)$$

²We choose this simplest case as an example. In fact, if we consider three families and three moduli, in order to avoid FCNC problems that might arise from the violation of the universal scalar

$$\hat{K} = -\ln [S + \bar{S}] - 3 \ln [T + \bar{T}] , \quad (21)$$

$$\tilde{K} = \left(\frac{3}{T + \bar{T}} + \frac{\alpha}{S + \bar{S}} \right) |C|^2 , \quad (22)$$

$$Re f_{\alpha\beta}^O = Re(S + \alpha T) \delta_{\alpha\beta} , \quad (23)$$

$$Re f_{\alpha\beta}^H = Re(S - \alpha T) \delta_{\alpha\beta} , \quad (24)$$

$$W = d_{xyz} C^x C^y C^z , \quad (25)$$

where S , T and C are dilaton, moduli and matter fields respectively. α is a next order correction constant which is related to the Calabi-Yau manifold. And the nonperturbative superpotential in the simplest model is [18]:

$$W_{np} = h \exp\left(-\frac{8\pi^2}{C_2(Q)}(S - \alpha T)\right) , \quad (26)$$

where the group in the hidden sector is Q and $C_2(Q)$ is the quadratic Casimir of Q . And in this case, Q is E_8 and $C_2(Q) = 30$.

With those information, we have following soft terms[14]:

$$M_{1/2} = \frac{\sqrt{3}M_{3/2}}{1+x}(\sin\theta + \frac{x}{\sqrt{3}}\cos\theta) , \quad (27)$$

$$\begin{aligned} M_0^2 &= M_{3/2}^2 - \frac{3M_{3/2}^2}{(3+x)^2}(x(6+x)\sin^2\theta + \\ &\quad (3+2x)\cos^2\theta - 2\sqrt{3}x \sin\theta \cos\theta) , \end{aligned} \quad (28)$$

$$A = -\frac{\sqrt{3}M_{3/2}}{(3+x)}((3-2x)\sin\theta + \sqrt{3}x \cos\theta) , \quad (29)$$

where $M_{3/2}$ is the gravitino mass, the quantity x defined above can be also expressed as

$$x = \frac{\alpha(T + \bar{T})}{S + \bar{S}} , \quad (30)$$

masses in three families (although this kind of the violation might be very small), we need to assume that [14]:

$$\alpha_1(T_1 + \bar{T}_1) = \alpha_2(T_2 + \bar{T}_2) = \alpha_3(T_3 + \bar{T}_3) , \quad (19)$$

where α_i $i=1, 2, 3$ are the next order correction constants. Then, the final soft terms will be the same as the simplest case if one consider the hidden sector gaugino condensation in the meantime, so, it is reasonable to choose the simplest case as an example to analyze the phenomenology.

and the angle θ is defined by:

$$\tan\theta = \frac{1}{\sqrt{3}} \frac{1 + \frac{2\pi}{C_2(Q)}(\alpha_{GUT}^{-1} + \alpha_H^{-1})}{1 - \frac{2\pi}{3C_2(Q)}(\alpha_{GUT}^{-1} - \alpha_H^{-1})}. \quad (31)$$

so, the soft terms $M_{1/2}$, M_0 , and A are the functions of the gravitino mass and the gauge coupling (α_H) in the hidden sector. Because the scalar mass M_0 should be larger than zero, the range of α_H is small, which is also important to keep the gaugino condensation scale low.

Because the range of the α_H is small, from 0.04 to 0.18, we pick two points as representatives: $\alpha_H = 0.05$ and $\alpha_H = 0.15$, which correspond to the dilaton dominant scenario and scalar quasi-massless scenario respectively [14].

In a realistic model, the gauge group in the hidden sector might not be E_8 , If one consider E_6 as the gauge group in the hidden sector, the quadratic Casimir of E_6 is 12. In this case that α_H can not be larger than 0.151, and the scalar quasi-massless scenario is [14]:

$$M_{1/2} = 0.989M_{3/2}; \quad M_0 = 0.008M_{3/2}; \quad (32)$$

$$A = -0.761M_{3/2}, \quad \alpha_H = 0.1522. \quad (33)$$

In comparison, the dilaton dominant SUSY breaking in this case is:

$$M_{1/2} = 1.534M_{3/2}; \quad M_0 = 0.870M_{3/2}; \quad (34)$$

$$A = -1.517M_{3/2}, \quad \alpha_H = 0.052. \quad (35)$$

4 Mass spectra and the permitted parameter space

We concentrate on the two typical supersymmetry breaking (SB) scenarios given in section 3 to calculate the low energy spectrum of superpartner and Higgs bosons masses: the scalar quasi-massless scenario corresponding to $m_0 = 8.09 \times 10^{-4}M_{1/2}$ and $A = -0.769M_{1/2}$ (see eqs.(32),(33)) and the dilaton dominant scenario corresponding to $m_0 = 0.567M_{1/2}$ and $A = -0.989M_{1/2}$ (see eqs.(34),(35)). In order to find out the effects of the supersymmetry breaking scales to low energy phenomenology, we take supersymmetry breaking scales Λ_{SUSY} as 2.0×10^{16} GeV (the GUT scale), 1×10^{15} GeV, and 1×10^{14} GeV. Those scales lower than 1×10^{14} GeV are not chosen because of the analysis in Section 2. But we will discuss their possible effects also.

We assume that the lightest supersymmetric particle (LSP) is the lightest neutralino and use several experimental limits to constraint the parameter space, including 1) the width of the decay $Z \rightarrow \chi_1^0 \chi_1^0$ is less than 8.4 MeV, and branching ratios of $Z \rightarrow \chi_1^0 \chi_2^0$ and $Z \rightarrow \chi_2^0 \chi_2^0$ are less than 2×10^{-5} , where χ_1^0 is the lightest neutralino and χ_2^0 is the other neutralino, 2) the mass of light neutral CP-even Higgs can not be lower than 77.7 GeV as the present experiments required, 3) the mass of lighter

chargino must be larger than 65.7 GeV as given by the Particle Data Group [28], 4) sneutrinos are larger than 43.1 GeV, 5) selectrons are larger than 58.0 GeV, 6) smuons larger than 55.6 GeV, 7) staus larger than 45.0 GeV.

We use ISAJET to do numerical calculations. In order to include all effects of bottom and tau Yukawa couplings, we made some modifications to ISAJET which are the same as those in Ref.[29]. We first examine the $M_{1/2}$ dependence of superpartner and Higgs boson masses in the two SUSY breaking scenarios. It is found that the masses increase when $M_{1/2}$ increase and $M_{1/2}$ should not be larger than 420 GeV if one demand the masses of superpartner and Higgs bosons are below 1 TeV. Then we scan boundaries of the parameter space in the two scenarios, taking $M_{1/2}$ from zero to 400 GeV. For a certain scenario, there are only two free parameters, $M_{1/2}$ and $\tan\beta$, as well as $\text{sign}(\mu)$ under the radiative electroweak symmetry breaking mechanism. The boundaries of the plane of the two parameters will be determined by the consistent conditions, such as the input should naturally trigger electric-weak symmetry breaking, the gauge unification, the Yukawa couplings are in the perturbative range, and there should be no tachyonic particles in mass spectrum, and by experimental limits above listed.

The results are shown in figure 1. The curves in figure 1 represent the upper bound and lower bound of $\tan\beta$ for each $M_{1/2}$, for two different SB scenarios, different Λ_{SUSY} . Figure 1a) draws the boundaries for $\mu < 0$, figure 1b) for $\mu > 0$. The dotted line represents Λ_{SUSY} equals 10^{14} GeV, the dashed line 10^{15} GeV, and the solid line the GUT scale, 2.0×10^{16} GeV. The curves marked 1 (2) are the boundaries of the parameter spaces in the quasi-massless scenario (the dilaton dominant scenario). For the scalar quasi-massless scenario, the permitted parameter spaces are the areas enclosed with closed boundaries, while for the dilaton dominant scenario, the permitted parameter spaces are not closed in right parts. The lower boundaries of $\tan\beta$ is about 1.6 for the dilaton dominant scenario. It is obvious from the figure 1 that for the scalar quasi-massless scenario, the parameter space is tightly constrained to the low mass spectrum and no large $\tan\beta$ region by consistent conditions, which is similar to that found in Refs. [11] and [20], while for the dilaton dominant scenario there is a much larger parameter space allowed.

The effect of sign of μ to the permitted parameter space is significant, as can be seen by comparing figure 1a) and figure 1b). For example, in the scalar quasi-massless scenario and $\Lambda_{SUSY}=10^{14}$ GeV, if $\mu < 0$, the parameter space is completely excluded. While as $\mu > 0$, there does exist an allowed region. The shape of boundaries of the parameter space for different sign of μ also claims the effect. But the effect in the dilaton dominant scenario is not as sensitive as in the quasi-massless scenario.

It is interesting that for the case of dilaton dominant scenario and $\mu < 0$, the lower boundary of $\tan\beta$ is singly determined by the experimental limit of light Higgs mass. If the limit increases, the lower boundary will increase correspondingly. It may be understood from the tree level formula of the mass of light Higgs. While the upper bound of $\tan\beta$ is determined by both some experimental limits and LSP condition. For example, when Λ_{SUSY} is 10^{14} GeV, $M_{1/2}$ from 84.7 GeV to 88.2 GeV, the upper bound is determined by the requirement that the mass of M_z should be less than $2m_{\tilde{u}_l}$, $2m_{\tilde{e}_l}$, $2m_{\tilde{e}_r}$, $2m_{\tilde{\tau}_1}$, $2m_{\tilde{b}_1}$, and $2m_{\tilde{t}_1}$; from 88.2 GeV to 102.0 GeV, it is determined by $m_{\chi_1^\pm} > 65.7$ GeV; from 102.0 GeV to 400 GeV, by LSP condition.

An interesting aspect of the allowed parameter space of the dilaton dominant scenario is that there exists a region where the mass spectrum is low while $\tan\beta$ is large. One can see from figure 1 that the region increases when Λ_{SUSY} decreases in the case of $\mu < 0$ and vice versa in the case of $\mu > 0$. We find that if the limit of the lightest chargino mass increases, the region will be reduced. We know $b \rightarrow s\gamma$ puts a very stringent constraint upon parameter space of MSSM. In the region, the charged Higgs mass is about 150 GeV and consequently it will lead to a significant contribution to $b \rightarrow s\gamma$. Therefore we would like to ask whether such a region can pass the constraint of $b \rightarrow s\gamma$. We will answer this question in the next section.

We illustrate the $\tan\beta$ dependence of mass spectra in the dilaton dominant scenario in figure 2, where we have chosen $M_{1/2}=120$ GeV. We have chosen this value of $M_{1/2}$ because it is in the region of the parameter space pointed out above and, as noticed in Ref.[29], a study of this point serves to nicely illustrate the importance of large $\tan\beta$ effects on Tevatron signals. Spectra are drawn in the same graph for $\mu > 0$ and $\mu < 0$ denoted by solid and dashed lines respectively. In figure 2a), the supersymmetry breaking scale is 10^{14} GeV, while in figure 2b), the scale is 1×10^{16} GeV. It is apparent that the mass spectrum will drop with the decrease of Λ_{SUSY} , just as given in Ref. [11], because the mass spectra depend on the length of the running scale of soft terms. The shorter the length, the lower the mass spectrum. This relation between the length of running scale and mass spectra will keep till the Λ_{SUSY} is lower than 10^9 GeV. It is evident from figure 2 that the sign of μ can effect the spectrum, though not significantly. It is also manifest from the figure that the upper bound of $\tan\beta$ is given by LSP condition. The figure vividly show the competition between the lightest neutralino and light stau for the LSP position. Another property worthy of mention is that masses of most sparticles are insensitive to $\tan\beta$ when $\tan\beta$ is large except $m_{\tilde{\tau}_1}$ m_{A^0} and m_{H^\pm} .

5 Constraints from $b \rightarrow s\gamma$

It is well known that $b \rightarrow s\gamma$ put a very stringent constraint on parameter space of various models. In this section we analyze the constraints from $b \rightarrow s\gamma$ on the permitted parameter space discussed in the last section. It is known long ago that supersymmetric contribution can interfere either constructively or destructively[32, 33, 34, 35, 36], which is determined by the sign of μ . For $\mu < 0$, the SUSY contribution interferes destructively with the Higgs's and W's contributions. With the spectrum of sparticles low, both charged Higgs and supersymmetric particles can largely contribute to the process. So even if the charged Higgs has large contributions, the supersymmetric contribution will cancel its effect and, for large $\tan\beta$, can even overwhelm its and W's contributions and force the C_7 (C_7 is the Wilson coefficient of the operator O_7 in the effective Hamiltonian, eq.(36), and the branching ratio of $b \rightarrow s\gamma$ is determined by $|C_7|^2$.) to change sign from positive to negative while keep the branch ratio still safely stayed in the bounds of experiments.

As we pointed out in the last section, there exists a region where the mass spectrum is low while $\tan\beta$ is large. It is known that supersymmetric contribution is proportional to $\tan\beta$ in the region. So it is expected that in this region supersym-

metric contribution will be very large.

Figure 3 is devoted to show $b \rightarrow s\gamma$ constraint. The curves in figure 3a) which have a dip correspond to the upper limit of $\tan\beta$, while the other correspond to lower limit of $\tan\beta$. The curves in figure 3b) which have a convex correspond to the upper limit of $\tan\beta$, while the other correspond the lower limit of $\tan\beta$. The experimental bounds of $b \rightarrow s\gamma$ are translated into the bounds of C_7 . But it should be reminded that C_7 can be either negative or positive. So we map the allowed parameter space into the plane of $M_{1/2}$ and C_7 . Figure 3a) is for $\mu < 0$. It is apparent that for $\Lambda_{SUSY} = 2 \times 10^{16}$ GeV most of the allowed region of the quasi-massless scenario can safely pass the experimental constraint due to the cancellation of the supersymmetric contribution to that of charged Higgs bosons when $\tan\beta$ increases as shown by the line corresponding to the upper limit of $\tan\beta$, except for some part close to the small $\tan\beta$ boundary, where charged Higgs contributes much, while supersymmetric particles contribute less since $\tan\beta$ is small. For the dilaton dominant scenario and Λ_{SUSY} equals 2×10^{16} GeV, we can see from figure 3a) that a quite large region is outside the experimental bound. This is because in the region SUSY contribution is not large enough to make C_7 still in experimental bound after cancelling out contributions of charged Higgs and W bosons. But for the case $\Lambda_{SUSY} = 10^{14}$ GeV, one can see from figure 3a) that there is a region where supersymmetric contribution indeed overwhelms charged Higgs's and W's contributions and makes C_7 change its sign. In this region $\tan\beta$ is large and the mass spectrum is low. This region has interesting phenomenology which have been analyzed in Ref.[29, 30, 31, 37, 38] and we shall discuss in the next section. Recently, in order to make more precise theoretical prediction, many literatures are devoted to NLO corrections of this process [39, 40, 41]. If we include the NLO corrections the region will decrease because, as pointed out in Ref. [40], the NLO correction of supersymmetric contribution decreases 30%, charged Higgs part decreases 20%, and SM part increases 10%.

Figure 3b) is devoted to $\mu > 0$. It is known that in such case the supersymmetric contribution interferes constructively. So the low mass spectrum region is not allowed whether $\tan\beta$ is large or small for both scenarios. One can see from the figure that for the quasi-massless scenario, all parameter space allowed in section II can not give the right prediction of $b \rightarrow s\gamma$ and is excluded by this strict constraint. For the dilaton dominant scenario, as $M_{1/2}$ increases to 330 GeV, the mass spectrum increases to such an extent that the region of low $\tan\beta$ enters into the experimental bound and is allowed. The typical mass of sparticle is about 500 GeV in this region.

For the dilaton dominant scenario and $\mu < 0$, it is possible to distinguish the interesting region where the mass spectrum is low and $\tan\beta$ is large from the region where the mass spectrum and $\tan\beta$ both are large. We shall discuss the possibility in an analysis of the rare decay $b \rightarrow s\tau^+\tau^-$.

6 Some phenomenological predictions

We now proceed to the analysis of low energy phenomenology. We shall discuss the rare decay $b \rightarrow s\tau^+\tau^-$ and Higgs boson productions $e^+e^- \rightarrow b\bar{b}H$. In order to search significant SUSY effects we shall concentrate on the case of the dilaton dominant

scenario and $\mu < 0$.

6.1 Decay $b \rightarrow s\tau^+\tau^-$

The effective Hamiltonian relevant to the $b \rightarrow sl^+l^-$ process is

$$H_{eff} = \frac{4G_F}{\sqrt{2}} V_{tb} V_{ts}^* \left(\sum_{i=1}^{10} C_i(\mu) O_i(\mu) + \sum_{i=1}^{10} C_{Q_i}(\mu) Q_i(\mu) \right) \quad (36)$$

where $O_i (i = 1, 2, \dots, 10)$ are given in Ref. [42], and Q_i 's come from exchanging neutral Higgs bosons and have been given in Ref. [43]. The coefficients $C_i(m_w)$ and $C_{Q_i}(m_w)$ in SUSYMs have been calculated [44, 45, 46, 30, 31]. The branching ratio and backward-forward (B-F) asymmetry for $b \rightarrow s\tau^+\tau^-$ depend on the coefficients C_7, C_8, C_9, C_{Q_1} and C_{Q_2} .

As pointed out in Ref.[30, 31], once C_{Q_1} and C_{Q_2} can compete with C_8 and C_9 , both invariant mass distribution and backward-forward asymmetry will be greatly modified. The values of C_{Q_1} and C_{Q_2} depend on the mass splitting and the mixing angle of stops, the masses of charginos and diagonalizing matrices U and V , the masses of neutral Higgs bosons, and $\tan^3\beta$ when $\tan\beta$ is large. For small masses of light chargino and neutral Higgs boson, large mass splitting of stops and large $\tan\beta$, C_{Q_1} and C_{Q_2} can be very large.

It is noted in the last section that, in the case of dilaton dominant scenario, $\mu < 0$ and $\Lambda_{SUSY}=10^{14}$ GeV, after taking into account the constraint of $b \rightarrow s\gamma$, there does exist a region (we shall call it the region A) of the parameter space where masses of sparticles are lower and $\tan\beta$ can up to 25. In figure 4, we map the allowed parameter space into C_{Q_1} and $M_{1/2}$ plane and C_{Q_2} and $M_{1/2}$ plane respectively. The lower boundary of $\tan\beta$ corresponds to the line near the $M_{1/2}$ -axis, while the upper boundary to the another line. It is obvious that the values of C_{Q_1} and C_{Q_2} indeed are very large in this region. We choose $M_{1/2}=110$ GeV and $\tan\beta=23$ as a representative point in the region and the values of C_{Q_i} ($i=1,2$) as well as C_i ($i=7,8,9$) at the point are tabulated in Table 1. It is also noticed in the last section that there is another region (we shall call it the region B) in the allowed parameter space where the mass spectrum and $\tan\beta$ both are large. In the region B, because $\tan\beta$ can be up to 33, C_{Q_1} and C_{Q_2} can also compete with C_8 and C_9 . But the values of C_{Q_1} and C_{Q_2} in this region are smaller when compared with those in the region A. In order to distinguish this region from the region A we have chosen $M_{1/2}=400$ GeV and $\tan\beta=31$ as a representative in this region to do calculations. The values of C_{Q_i} ($i=1,2$) and C_i ($i=7,8,9$) at the point are also tabulated in Table 1. One can see from the Table that a typical C_{Q_1} in the region A and is -16, while a typical C_{Q_1} in the region B is -4.5. Some masses of sparticles used in computations are listed in Table 2.

The numerical results of the invariant mass distribution and B-F asymmetry for the two sets of values of coefficients C_{Q_i} and C_i given in table 1 are shown in figure 5. It is obvious that the deviation from SM is very large for both cases, but for the set A the deviation is more drastic. The enhancement of the differential branching ratio $d\Gamma/ds$ in the case of set A can reach 400% compared to SM. Meanwhile, the difference between the set A and set B is also very significant so that one can distinguish them

from the measurements of $b \rightarrow s\tau^+\tau^-$. It should be noted that if without including the contributions of neutral Higgs, the deviation from SM is small.

	$M_{1/2}$	$\tan\beta$	C_7	C_8	C_9	C_{Q_1}	C_{Q_2}	$\text{BR}(b \rightarrow s\gamma)$
Set A	110	23	-0.25	-3.08	4.12	-16.64	16.36	2.14×10^{-4}
Set B	400	31	0.24	-3.06	4.50	-4.35	4.30	2.0×10^{-4}

Table 1: The values of C_{Q_i} (i=1,2) and C_i (i=7,8,9) for the chosen representative points in the regions A and B.

	$m_{\tilde{q}}$	$m_{\tilde{t}_1}$	$m_{\tilde{t}_2}$	m_{χ_1}	m_{χ_2}	m_{h_0}	m_{H^\pm}	$m_{\tilde{\tau}_1}$	$m_{\chi_1^0}$
Set A	246.30	162.95	336.86	73.58	192.56	103.13	153.31	50.18	50.16
Set B	797.60	575.75	784.00	332.08	512.48	116.68	464.21	206.67	206.60

Table 2: The masses of sparticles used in the computations for the chosen representative points in the regions A and B.

6.2 $e^+e^- \rightarrow b\bar{b}H$

The Higgs boson is the missing piece and also the least known one of the standard model and other supersymmetrical models. The pursuit of the Higgs bosons predicted by these models is one of the primary goals of the present and next generation of colliders. The Next Linear Collider(NLC) operating at a center-of-mass energy of $500 - 2000\text{GeV}$ with the luminosity of the order of $10^{33}\text{cm}^{-2}\text{s}^{-1}$ can provide an ideal place to search for the Higgs boson, since the events would be much cleaner than in the LHC and the parameters of the Higgs boson would be easier to extracted.

Based on the analysis in previous sections, we will present some data examples of the cross sections for the process $e^+e^- \rightarrow b\bar{b}H$ in this subsection. In figure 6 we show the SM Higgs production cross section as a function of the Higgs mass. In figure 7 and 8, we show the production cross sections as the function of the $\tan\beta$, where $M_{1/2} = 120\text{ GeV}$ and 400 GeV , respectively, and other parameters are depicted in figures captions. As usual, h^0 and H^0 denote the CP-even neutral Higgs bosons with $m_{h^0} < m_{H^0}$, respectively. It should be noticed that, as $M_{1/2} = 400\text{ GeV}$, the mass of H^0 is too heavy to be produced by the NLC when $\sqrt{s} = 500\text{ GeV}$. Comparing figures 7 and 8 with figure 6, it is evident that Higgs production cross sections increase significantly when $\tan\beta$ increases, as expected, except for $b\bar{b}h^0$ in the case of $M_{1/2}=400\text{ GeV}$. For the $b\bar{b}h^0$ production, the enhancement of large $\tan\beta$ is offset by the small

$\sin\alpha$ because in the case of $M_{1/2} = 400$ GeV, m_{h^0} is much smaller than masses of the other Higgs bosons.

7 Conclusions

We have revisited the the eleven dimension Planck scale, the physical scale of the eleventh dimension, the physical scale of Calabi-Yau manifold and coupling in hidden sector in M-theory on S^1/Z_2 and discussed the reasonable bounds on them under the ansatz that the scale of M_{GUT} , M_H and $[\pi\rho_p]^{-1}$ should be lower than the eleven dimension Planck scale. It has been shown that $\Lambda_{SUSY} \geq 10^{14}$ GeV if one assumes $\Lambda_{SUSY} = [\pi\rho_p]^{-1}$ [11]. We have analyzed the soft terms in the simplest compactification of M theory on S^1/Z . We have calculated sparticle spectra at different values of Λ_{SUSY} and found that the spectra lower when Λ_{SUSY} decrease. Therefore, compared with the spectra in the weakly coupling string models and general SUSY GUT models, the spectra in M theory phenomenology are lower, which is, of course, more easier to search at colliders. The LEP experiment and $b \rightarrow s\gamma$ constraints on the parameter space in the dilaton dominant and scalar quasi-massless supersymmetry breaking scenarios are analyzed. Finally, we give predictions for the rare decay $b \rightarrow s\tau^+\tau^-$ and neutral Higgs boson productions. An interesting result is that one could discover supersymmetry from $b \rightarrow s\tau^+\tau^-$ in future B factories if nature give us large $\tan\beta$ and low mass spectra which come out as a consequence of M theory low energy phenomenology.

8 Acknowledgements

This research was supported in part by the National Science Foundation of China. This research (T. Li) was supported in part by the U.S. Department of Energy under Grant No. DE-FG02-95ER40896 and in part by the University of Wisconsin Research Committee with funds granted by the Wisconsin Alumni Research Foundation.

References

- [1] For reviews see: J. H. Schwarz, Nucl. Phys. Proc. Suppl. **55B** (1997) 1; M. J. Duff, Int. J. Mod. Phys. **A11** (1996) 5623; "Fields, Strings, and Duality", (TASI 96), eds. C. Efthimiou and B. Greene, World Scientific, 1997.
- [2] P. Horava and E. Witten, Nucl. Phys. B **475** (1996) 94.
- [3] E. Witten, Nucl. Phys. B **471** (1996) 135.
- [4] P. Horava, Phys. Rev. D **54** (1996) 7561.
- [5] T. Banks and M. Dine, Nucl. Phys. B **479** (1996) 173 and hep-th/9609046.
- [6] K. Choi, Phys. Rev. D **56** (1997) 6588; K. Choi, H. B. Kim, H. Kim, hep-th/9808122.
- [7] I. Antoniadis and M. Quiros, Phys. Lett. B **392** (1997) 61.
- [8] I. Antoniadis and M. Quiros, hep-th/9705037, hep-th/9707208, hep-th/9709023.
- [9] E. Dudas and J. C. Grojean, hep-th/9704177; E. Dudas, hep-th/9709043.
- [10] E. Caceres, V. S. Kaplunovsky and I. M. Mandelberg, Nucl. Phys. B **493** (1997) 73.
- [11] T. Li, J. L. Lopez and D. V. Nanopoulos, hep-ph/9702237, Mod. Phys. Lett. A. **12** (1997) 2647.
- [12] T. Li, J. L. Lopez and D. V. Nanopoulos, Phys. Rev. D **56** (1997) 2602.
- [13] T. Li, Phys. Rev. D **57** (1998) 7539.
- [14] T. Li, hep-th/9804243.
- [15] H. P. Nilles, M. Olechowski and M. Yamguchi, hep-th/9707143, Phys. Lett. B **415** 415 (1997) 24; hep-th/9801030.
- [16] Z. Lalak and S. Thomas, hep-th/9707223.
- [17] A. Lukas, B. A. Ovrut and D. Waldram, hep-th/9710208, hep-th/9803235.
- [18] A. Lukas, B. A. Ovrut and D. Waldram, hep-th/9711197.
- [19] K. Choi, H. B. Kim and C. Munoz, hep-th/9711158.
- [20] D. Bailin, G. V. Kraniotis and A. Love, hep-ph/9803274.
- [21] J. Ellis, A. E. Faraggi and D. V. Nanopolous, hep-th/9709049.
- [22] E. Dudas and J. Mourad, hep-th/9701048.
- [23] K. Benakli, hep-th/9805181.
- [24] Z. Lalak, S. Pokorski, S. Thomas, hep-ph/9807503.
- [25] A. Lukas, B. A. Ovrut, D. Waldram, hep-th/9808101.
- [26] D. V. Nanopolous, hep-th/9711080.
- [27] D. Bailin, G.V. Kraniotis, and A. Love, hep-ph/9803274.

- [28] Particle Data Group, Review of Particle Physics, *Europ. Phys. J.* **C3** (1998) 1.
- [29] H. Baer, C.-H. Chen, M. Drees, F. Paige, and X. Tata, *Phys. Rev. Lett.* **79** (1997) 986.
- [30] Chao-shang Huang and Qi-shu Yan, hep-ph/9803366, to appear in *Phys. Lett. B*.
- [31] Chao-shang Huang, Wei Liao, and Qi-shu Yan, hep-ph/9803460, to appear in *Rapid Communications of Phys. Rev. D*.
- [32] J.L. Lopez, D.V. Nanopoulos, X. Wang and A. Zichichi, *Phys. Rev. D* 51(1995) 147.
- [33] R. Barbieri and G.F. Giudice *Phys Lett B* 309(1993)86.
- [34] M.A. Diaz, *Phys. Lett. B* 322 (1994) 591.
- [35] T. Goto and Y. Okada, *Prog. of Theor. Phys.* 94 (1995) 407.
- [36] R. Garisto and J. N. Ng *Phys. Lett. B* 315 (1993) 372.
- [37] H. Baer, C.-H. Chen, M. Drees, F. Paige, and X. Tata, hep-ph/9809223.
- [38] W. Loinaz and J. D. Wells, hep-ph/9808287.
- [39] M. Neubert, hep-ph/9809377.
- [40] M. Ciuchini et al., hep-ph/9806308.
- [41] A. L. Kagan and M. Neubert, hep-ph/9805303.
- [42] B. Grinstein, M.J. Savage and M.B. Wise, *Nucl. Phys. B* 319 (1989) 271.
- [43] Y.B. Dai, C.S. Huang and H.W. Huang, *Phys. Lett. B* 390 (1997) 257.
- [44] S. Bertolini, F. Borzumati, A. Masieso and G. Ridolfi, *Nucl. Phys. B* 353 (1991) 591.
- [45] P. Cho, M. Misiak and D. Wlyer, *Phys. Rev. D* 54 (1996) 3329.
- [46] T. Goto, Y. Okada, Y. Shimizu and M. Tanaka, *Phys. Rev. D* 55 (1997) 4273.

Figure Captions

Fig. 1:

The upper and lower bounds of $\tan\beta$ vary with $M_{1/2}$, for the dilaton dominant and scalar quasi-massless scenarios and for different values of Λ_{SUSY} . The curve labeled 1(2) represents the scalar quasi-massless (dilaton dominant) scenario. The dotted line is for $\Lambda_{SUSY} = 10^{14}$ GeV, the dashed line 10^{15} GeV, and the solid line the GUT scale, 2×10^{16} GeV. For the scalar quasi-massless scenario, the permitted parameter spaces are with closed boundaries, while for the dilaton dominant scenario, the permitted parameter spaces are not closed in right parts. Fig. 1a) is for $\mu < 0$,

fig. 1b) is for $\mu > 0$. The lower bound of $\tan\beta$ is about 1.6 for the dilaton dominant scenario.

Fig. 2:

Computed values of sparticle masses versus $\tan\beta$ for $M_{1/2}=120$ GeV. Fig. 2a) is for $\Lambda_{SUSY} = 10^{14}$ GeV and Fig. 2b) 1×10^{16} GeV. The solid (dashed) lines represent $\mu > (<)0$.

Fig. 3:

The variation of C_7 with $M_{1/2}$ and $\tan\beta$, scenarios and Λ_{SUSY} . The solid lines represent $\Lambda_{SUSY} = 2 \times 10^{16}$ GeV, the dotted lines represent $\Lambda_{SUSY} = 1 \times 10^{14}$ GeV. The curve labeled 1 (2) represents the scalar quasi-massless (dilaton dominant) scenario. Fig. 3a) is devoted for the case $\mu < 0$, fig. 3b) for the case $\mu > 0$. The experimental constraints of $b \rightarrow s\gamma$ have been translated to the constraints on C_7 , which are represented by two sets of parallel horizontal lines. The curves in figure 3a) which have a dip correspond to the upper limit of $\tan\beta$, while the other correspond to lower limit of $\tan\beta$. The curves in figure 3b) which have a convex correspond to the upper limit of $\tan\beta$, while the other correspond to the lower limit of $\tan\beta$.

Fig. 4:

For the case of the dilaton dominant scenario, $\mu < 0$ and $\Lambda_{SUSY}=10^{14}$ GeV, the variation of C_{Q_1} and C_{Q_2} with $M_{1/2}$ and $\tan\beta$. We map the permitted parameter space plane into C_{Q_i} and $M_{1/2}$ planes. The lower boundary of $\tan\beta$ corresponds to the line near the $M_{1/2}$ -axis, while the upper boundary to the another line.

Fig. 5:

The branching ratio multiplied by $10^{(-6)}$ for the process $b \rightarrow s\tau^+\tau^-$ versus s where $s = \frac{(p_+ + p_-)^2}{m_b^2}$ and p_+ (p_-) is the four momentum of τ^+ (τ^-). The related coefficients and masses are listed in table 1 and table 2 respectively. The solid line is for SM prediction, the dashed line corresponding to the prediction of set A, the dotted line the prediction of set B. We find if without including the contributions of neutral Higgs bosons, the deviation from SM is small.

Fig. 6:

The cross sections of the process $e^+e^- \rightarrow b\bar{b}H$ as a function of the mass of Standard Model Higgs m_H .

Fig. 7:

The cross sections of the process $e^+e^- \rightarrow b\bar{b}H(H = h^0, H^0)$ as a function of $\tan\beta$, where $M_{1/2} = 120$ GeV, $\Lambda_{SUSY} = 10^{14}$ GeV and $Sign(\mu) = -1$ in the dilaton dominant scenario.

Fig. 8:

Same with figure 7 but $M_{1/2} = 400$ GeV.

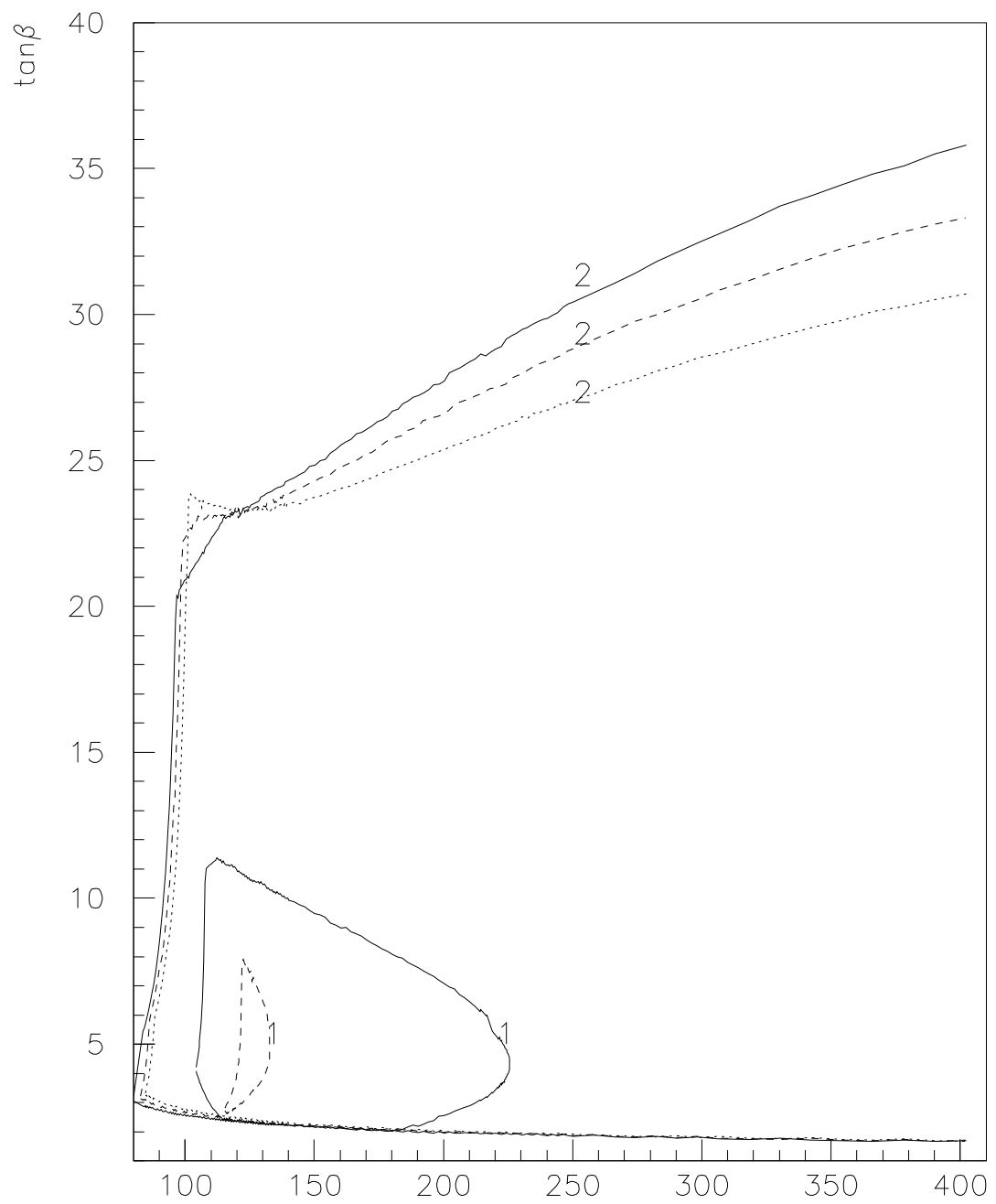


Fig. 1a, $\mu < 0$ $m_{1/2}$

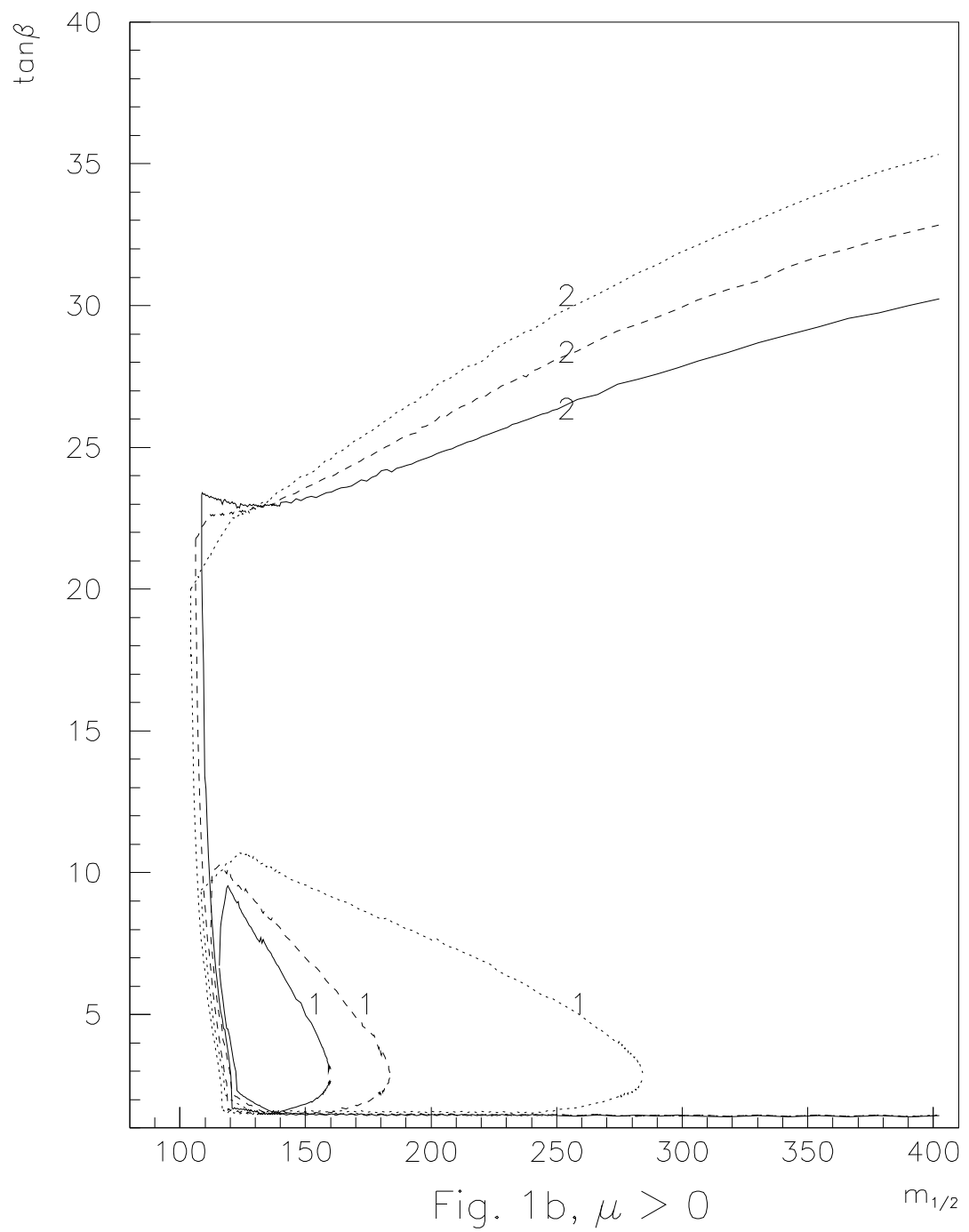
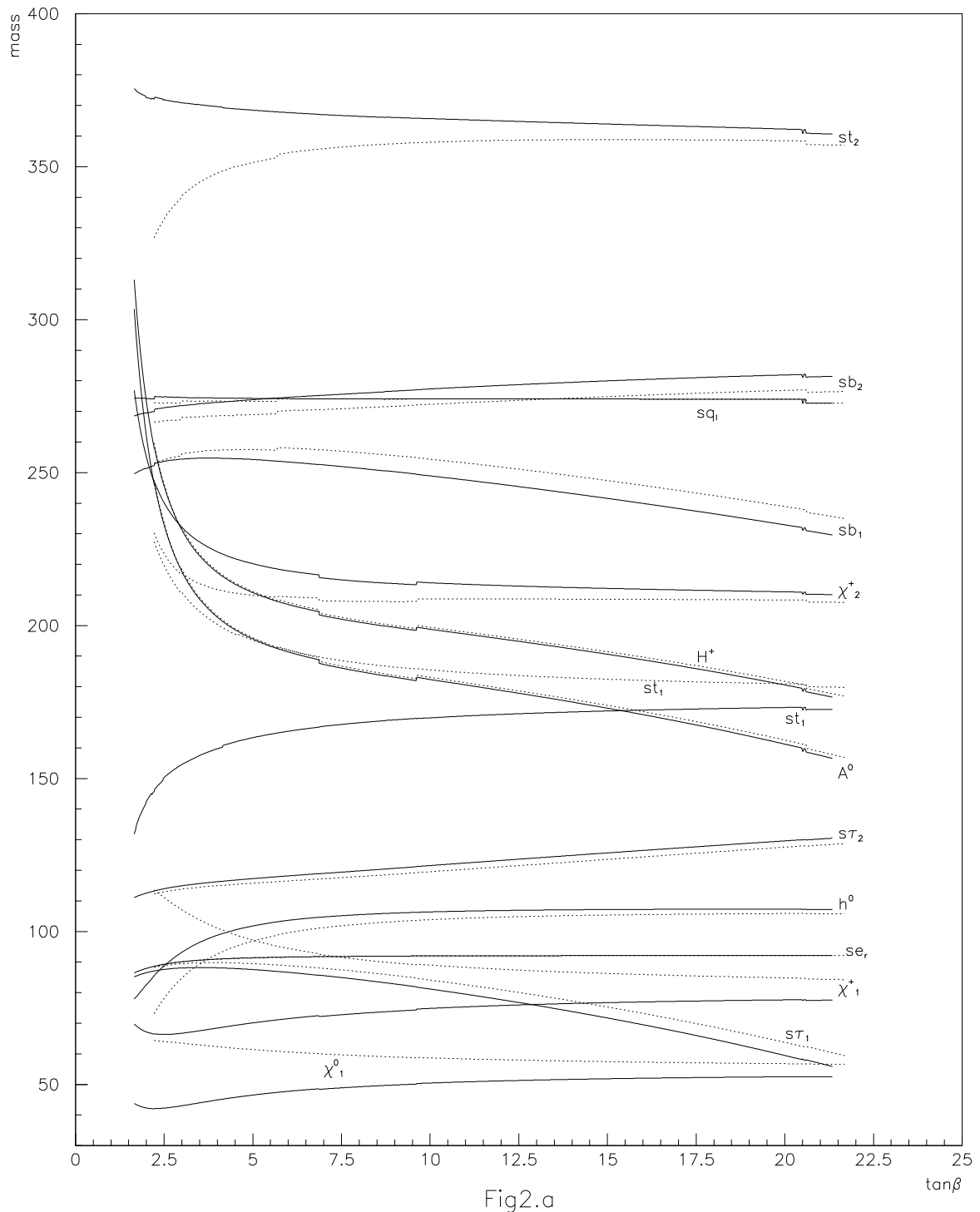
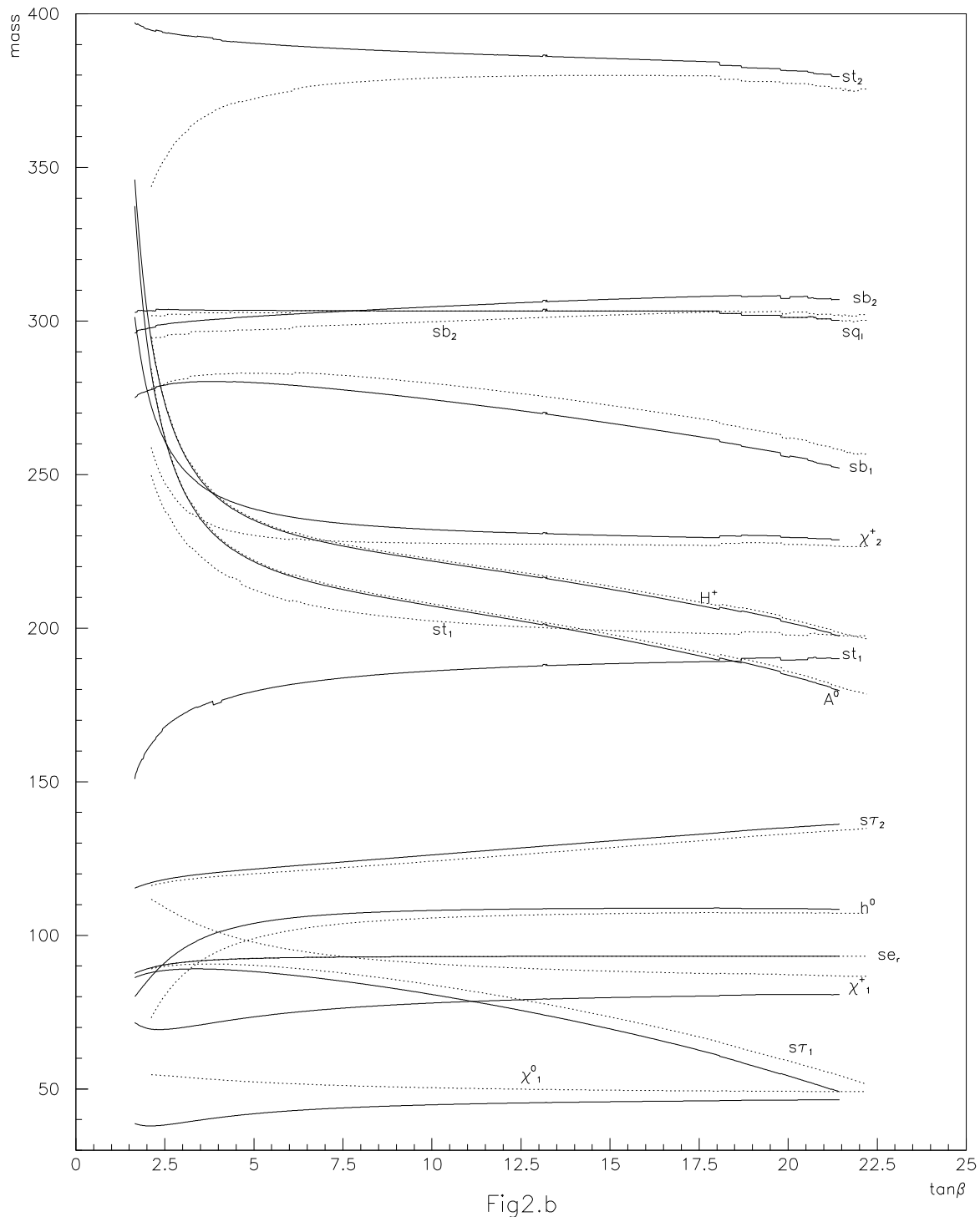


Fig. 1b, $\mu > 0$





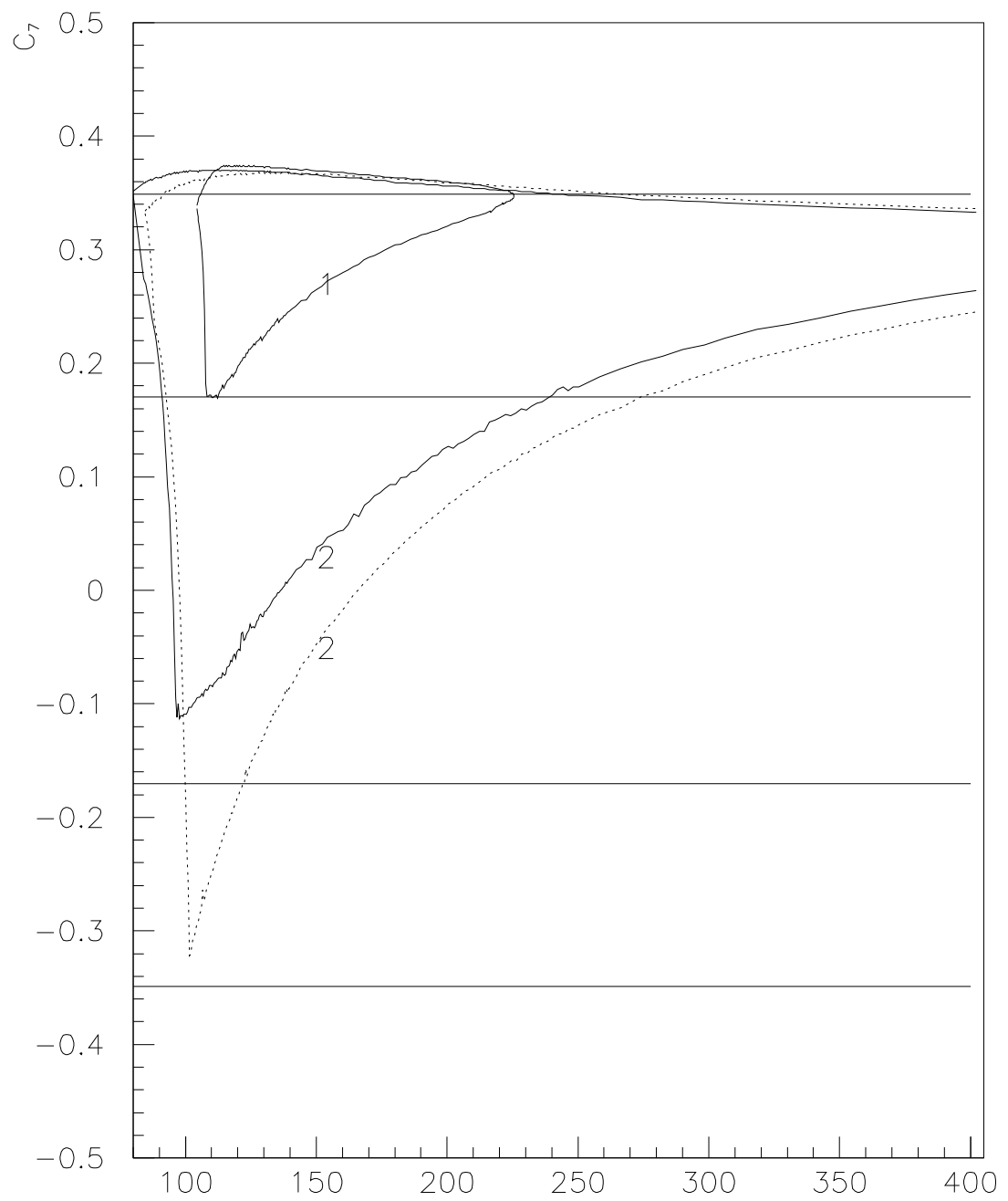


Fig 3a, $\mu < 0$ $m_{1/2}$

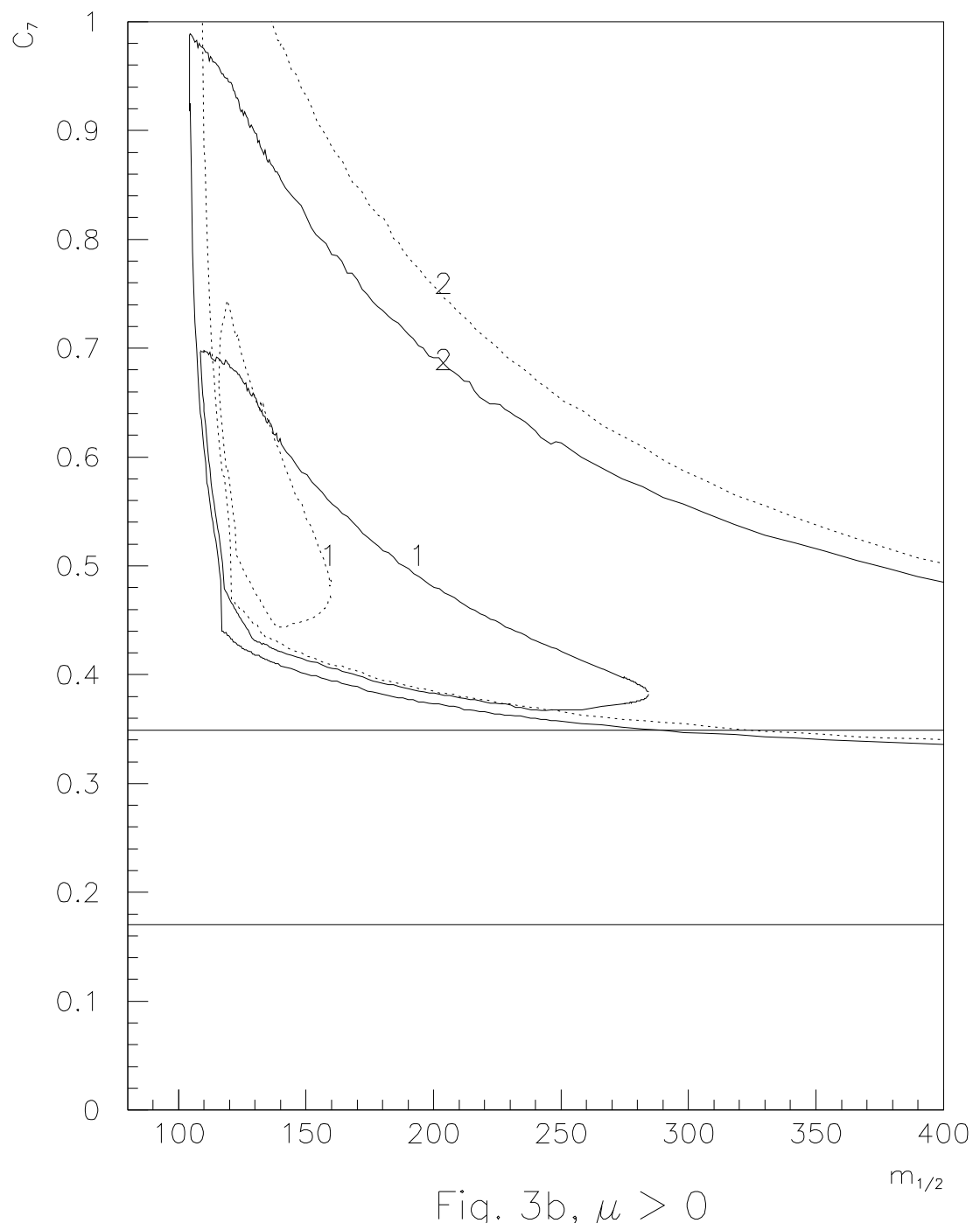


Fig. 3b, $\mu > 0$

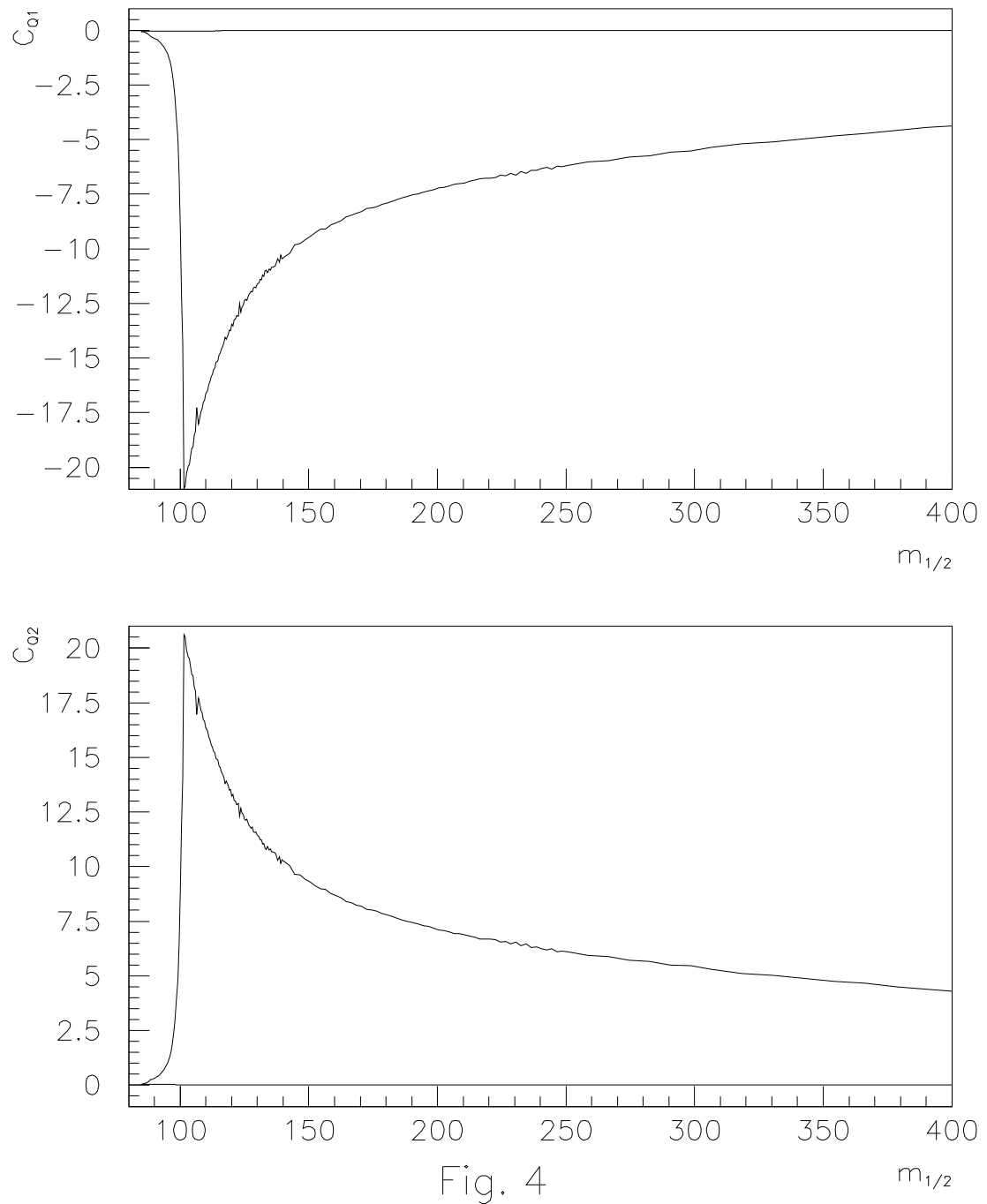


Fig. 4

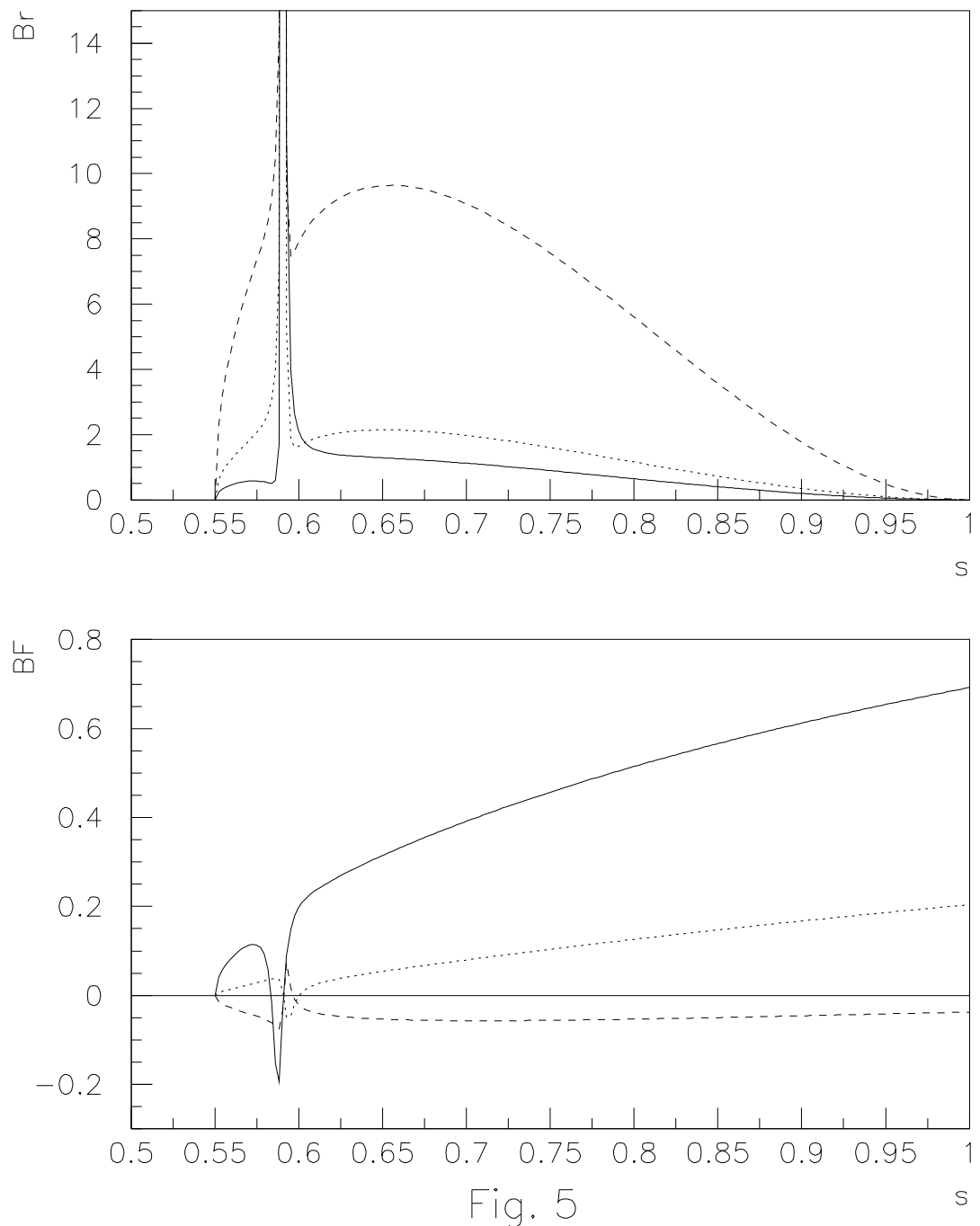


Fig. 5

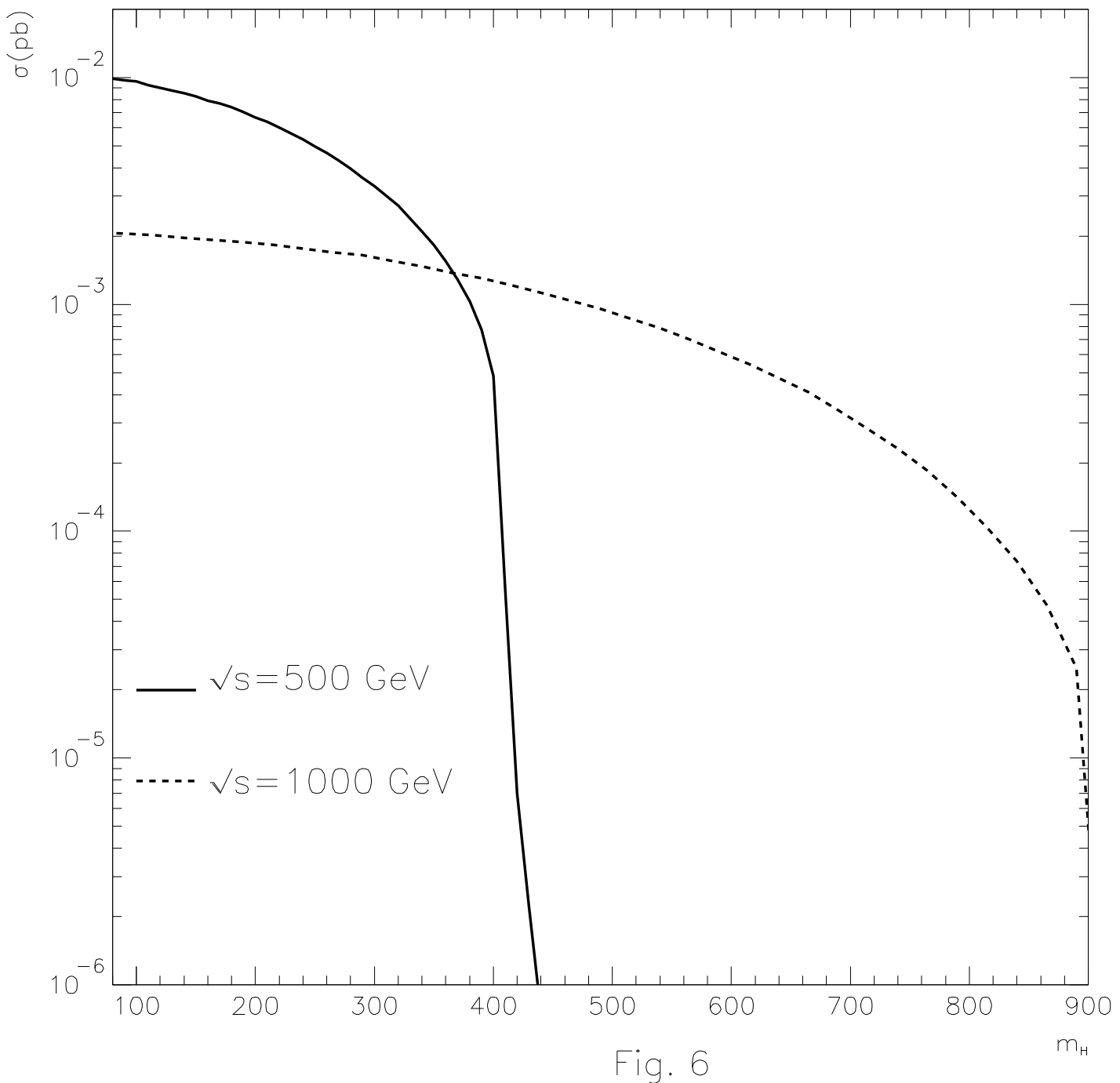


Fig. 6

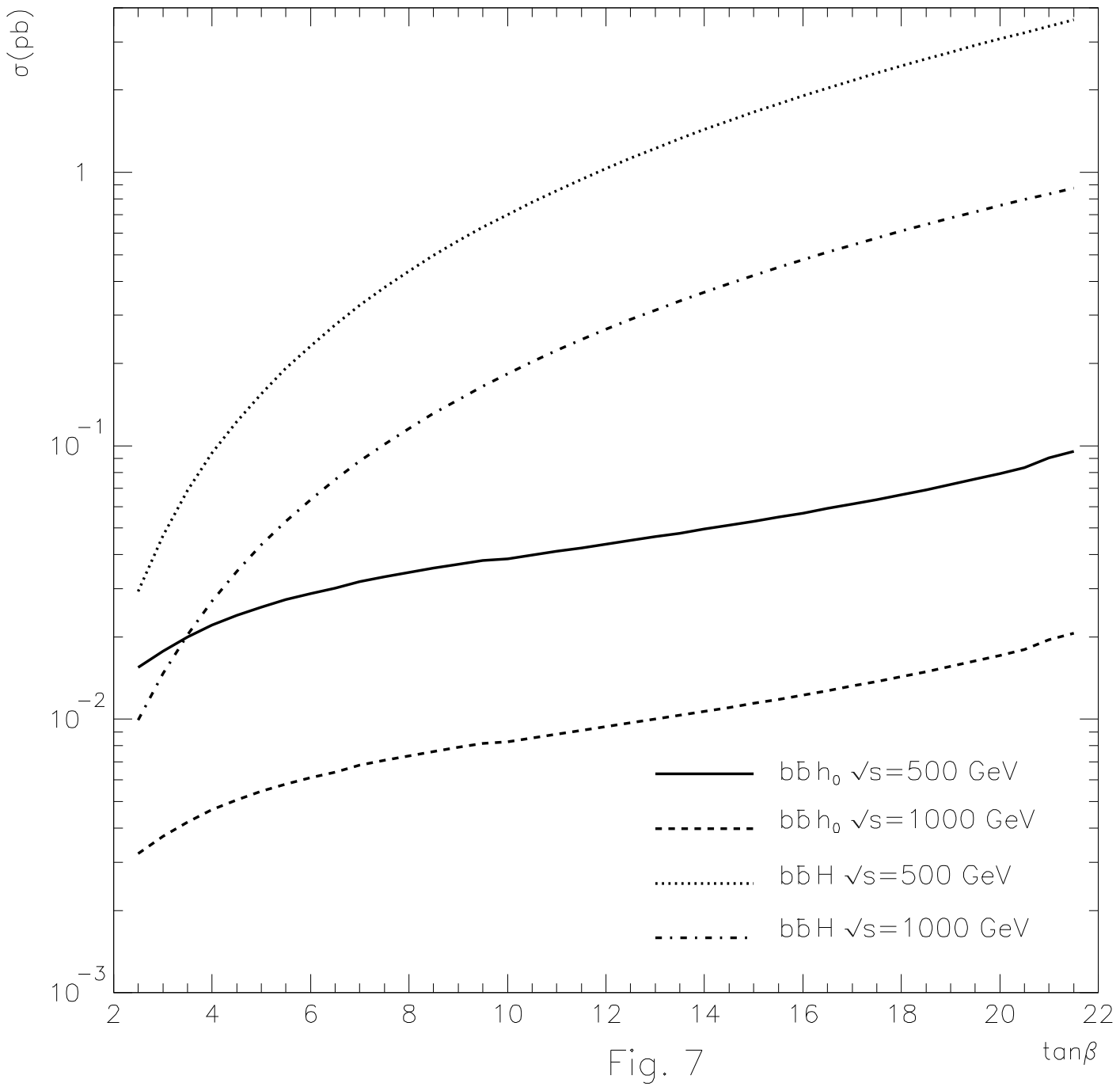


Fig. 7

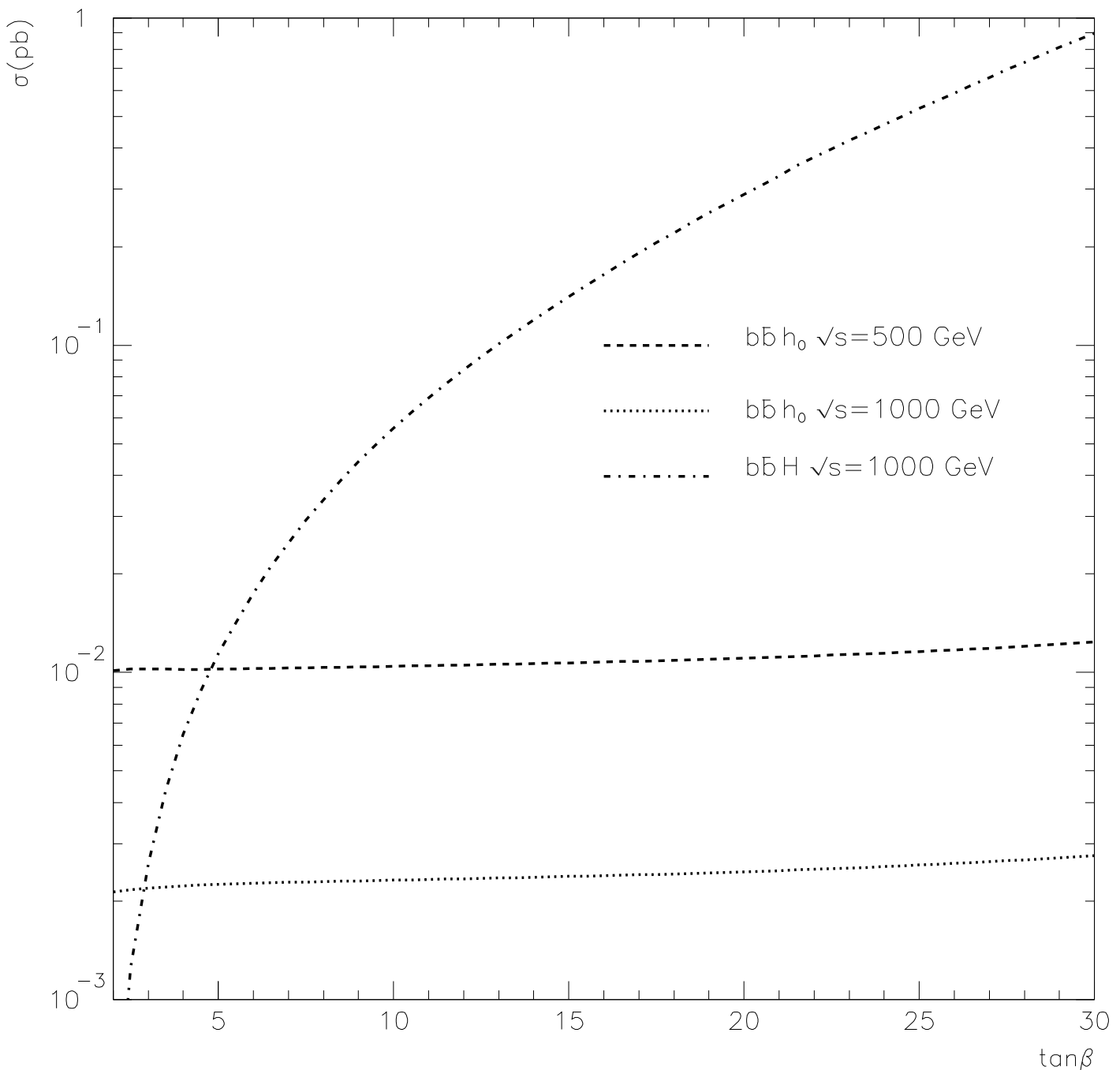


Fig. 8